Journal of Crystal Growth 65 (1983) 105–123
North-Holland, Amsterdam

CONVECTIVE TRANSPORT IN VAPOR GROWTH SYSTEMS

G.H. WESTPHAL

Texas Instuments Incorporated, P.O. Box 225936, MS 147, Dallas, Texas 75265, USA

The interaction of gravity with fluid density gradients greatly influences mass and heat transfer in vapor growth systems. These affects are reviewed by discussing specific examples of closed and open tube chemical or physical vapor transport systems. Both theoretical analysis and experimental results are presented. Emphasis is placed on the closed tube systems since they are often the best characterized and are the best initial candidates for study in a low-g environment (e.g., space). The open tube systems discussed include halide vapor phase epitaxy of GaAs and the endothermic (cold wall) epitaxial process for Si. The convective stability criteria for open tubes are reviewed and a guide to the mass transfer literature is presented. For terrestrial closed tube systems, two recent results are of particular significance. First, laser Doppler anemometry experiments have demonstrated a complicated detailed flow pattern near the crystal interface. Presumably this effect can strongly influence crystal homogeneity. Second, numerical calculations have shown the well known Klosse and Ullersma transport rate calculations [J. Crystal Growth 18 (1973) 167] to be correct only at low Grashof numbers and that such closed tube transport is also Prandtl number dependent.

1. Introduction

Crystallization from vapors is the method of choice for the preparation of many technologically important materials. Open tube vapor phase epitaxial processes, for example, are in wide spread use for the growth of thin films of Si and GaAs. Closed tube (ampoule) vapor growth is often used for the preparation of bulk samples, such as CdS.

Because vapor crystal growth usually occurs at temperatures lower than those of other growth techniques that might be used for the same material, it has certain advantages. For instance, materials that decompose before melting, have adverse melt/container reactions, or have a high temperature solid/solid phase transition can often be grown at lower temperatures. Also, the low atomic roughness of the vapor-solid interface implies strong morphological stability in the presence of heat and mass transfer non-uniformities. For epitaxial processes, enhanced capability is provided by the ability to vary the vapor composition over a wide range and to grow on larger area wafers than are normally used in liquid phase epitaxy.

The main disadvantages of vapor growth are parasitic nucleation and low growth rates. As pointed out in ref. [1], however, these difficulties are seldom due to intrinsic limitations, such as slow interfacial kinetics. Lack of appropriate heat and mass transfer is typically the problem. In most vapor growth systems high mass transport rates can be achieved. But feasible growth rates are frequently limited by the most commonly used experimental conditions.

Vapor growth may be divided into four categories, as shown in fig. 1. Physical vapor transport (PVT), or sublimation–condensation, is a closed tube technique that may be used to grow crystals if the material vapor pressure exceeds 10^{-2} torr at some feasible temperature. If the vapor pressure is too low at convenient temperatures to allow effective transport by PVT, then growth by chemical vapor transport (CVT) may be possible. In this closed tube technique a reversible chemical reaction, which yields only gaseous products, is used to volitilize the starting material.

Occasionally physical vapor deposition (PVD), i.e. open tube sublimation–condensation, has been used to grow bulk crystals [2]. The most commonly used vapor growth technique however, is chemical vapor deposition (CVD). Here a chemical reaction is combined with open flow to effect transport. The reaction may either be reversible (GaAs, halide

0022-0248/83/$03.00

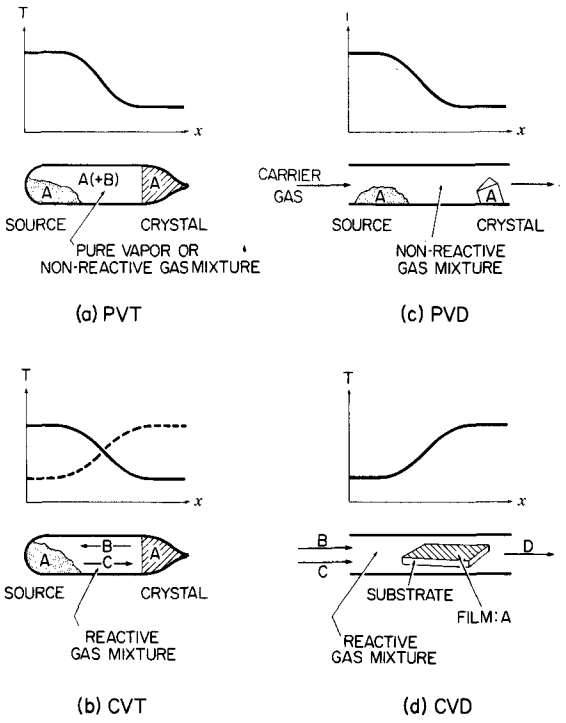

Fig. 1. Methods for crystal growth from vapors, and corresponding temperature profiles (schematic): (a) physical vapor transport: sublimation and recrystallization of component A in temperature gradient; (b) chemical vapor transport: reaction of solid A with vapor B to volatile product(s), here C, and back-reaction to solid A in zone of different temperature; solid and dashed $T(x)$ for endothermic and exothermic transport reaction respectively; (c) physical vapor deposition: transfer of subliming A by (saturated) carrier gas to colder growth area; (d) chemical vapor deposition: reaction of gases (vapors), e.g. B and C, blown into hot zone to form solid A and gaseous products, e.g. D. After ref. [1].

epi) or irreversible (Si, chlorosilane) at the deposition temperature.

The usefulness of these vapor grown materials often depends critically on their compositional uniformity. Local variations in dopant level or material stoichiometry can, for example, strongly influence the performance of an electronic or optical device. Compositional uniformity, however, requires homogeneous and steady-state heat and mass transfer at the crystal vapor interface. If crystallization occurs from a fluid phase, then the exact state at the growth interface depends on the conditions in the bulk fluid. Thus knowledge of the fluid motion is essential to an understanding of the crystal uniformity to be expected from a given set of (growth system) boundary conditions. For a discussion of the basic effects of fluid homogeneity on crystal quality, see ref. [1].

In a fluid, heat and mass transfer is accomplished mainly by convection. Convection is the transport of energy and mass by a medium involving movement of the medium itself. Heat transfer can occur by conduction (no movement of the medium) but, only rarely, does mass transfer entirely avoid convection. This is because mass transfer by diffusion is not strictly analogous to heat conduction. As heat is conducted, energy is transferred but the molecules involved remain near their time averaged space coordinates. Therefore, the mass-connected reference frame, with respect to which the conductive heat flux is expressed, remains stationary, unless a convective motion is imposed by external means. As mass diffuses, however, under most circumstances the (same) mass centered reference frame with respect to which the diffusion mass flux is expressed is itself moving due only to the diffusive mass flow. This diffusive induced fluid motion is called the advective flux (for a complete description, see ref. [3]).

In virtually all crystal growth systems, the (fluid phase) nutrient from which the crystal is grown has a different composition than the crystal. Even PVT or growth from ostensibly pure melts usually involves some segregation at the interface. Thus convection, especially to the extent that it involves mixing of fluid elements of different composition or temperature distribution, strongly effects crystal uniformity and growth rate.

Convection is often classified according to its origin. Advection, as mentioned above, arises as a consequence of diffusive mass transfer. Fluid density gradients can interact with body forces, the most common of which is gravity, to produce "natural" or "free" convection. The density gradients may be caused by thermal expansion or concentration gradients arising from, for example, the temperature dependence of chemical equilibrium. Forced convection usually arises from an external input of mechanical energy such as stirring or the establishment of a pressure gradient in an open

flow system. Convection is further classified as steady or non-stady (time dependent).

Convection per se is not undesirable in crystal growth systems. It can substantially increase growth rates. Yet it can also cause severe non-uniformities. Thus it is uncontrolled convection that is to be avoided. It is the purpose of this review to describe convective effects in closed and open tube vapor growth systems and indicate how a knowledge of convection may be used to advantage. Emphasis will be placed on steady state convection in closed ampoules. Closed tube geometries are much simpler than most open tube ones (especially those of silicon epitaxy) and considerable theoretical analysis and numerical modeling have been done on ampoule systems. Also, because of the compactness of these systems, they are the most likely candidates for initial study in a microgravity environment (i.e. space). Open tube convection, however, will also be reviewed. Time dependent convection will be discussed in relation to the open flow systems.

2. Convective effects in closed tubes (ampoules)

2.1. Steady state convection, analysis

Analysis of convective vapor transport in closed ampoules has been the subject of several recent reviews [1,4,5]. The most widely used model for diffusive–convective transport in horizontal ampoules is due to Klosse and Ullersma [6] (hereinafter referred to as KU). Nevertheless, various experimental studies have failed to quantitatively confirm KU's prediction for a significant range of characteristic parameters (see, e.g., refs. [7,8]). In recent numerical modeling efforts [9,10] the simplifying assumptions of KU's analysis have been relaxed and the range of fluid parameters investigated has been greatly extended. The work of Markham and Rosenberger [10], in particular, seems to be the most thorough analyses of closed ampoule convection currently available and what follows is adapted largely from it.

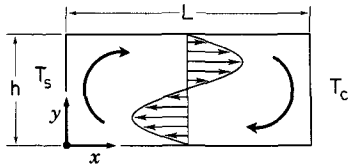

Fig. 2. Schematic representation of the channel geometry used to model convection in an ampoule. After ref. [10].

Since the numerical results are compared to KU's model, a brief description of their work is given here. The ampoule transport is modeled using a rectangular horizontal cavity of height, h, and length, l, as shown in fig. 2. The depth is assumed to be very large compared to h or l. Expansive convection is driven by differentially heating the two vertical walls. The end walls also form the interfaces between the solid source, the vapor, and the crystal. Heat transfer is not considered and linear temperature and mass density profiles are assumed. The linear temperature profile implies that the vapor has infinite thermal conductivity and therefore, a vanishingly small Prandtl number (Pr) (see nomenclature at end of paper). Also, velocity contributions arising from net mass transfer (interfacial flow) are neglected.

The convective flow is then obtained by assuming a stream function for an infinitely long horizontal channel with symmetric antiparallel flow (shaped profile of fig. 2). The boundary conditions for the vertical end walls are matched to the stream function with adjustable parameters which are determined by a variational technique. This newly found velocity distribution is then used to solve the concentration profile. The final result describes the enhancement of mass transport due to convection in the form of a simple mathematical relation involving the aspect ratio ($AR = l/h$), the Grashof number (Gr), and the Schmidt number (Sc). No solutions for local variations in the concentration distribution and growth flux were determined.

The numerical model of ref. [10] assumes a geometry identical to that of KU. In addition it is assumed that a component A sublimes from the solid source, is transported through and with a non-active component B, and condenses at the crystal interface. B is completely rejected and A is in equilibrium at each interface. The boundary walls are assumed to be impermeable to both components and thermally ideally conducting.

Radiative heat transfer is neglected. The molecular weight of the two vapor components are assumed equal, so that the model is restricted to thermal expansive convection. Also, frictional contributions to the energy transport are ignored. The velocity and binary diffusivity are assumed concentration and temperature independent, and are evaluated at the average temperature.

The transport in the cavity is governed by the system of nonlinear, coupled conservation equations for momentum (Navier–Stokes), mass (continuity), species (diffusion) and energy (for a full description of these equations, see refs. [3] or [11]). The so called compressible terms are kept in the momentum transport equation. Also, neither creeping flow nor boundary layer assumptions are made. Ideal gas behavior is assumed, but the total pressure is not constrained to a fixed value.

The no-slip condition is assumed at all solid surfaces and the end walls are assumed to have a uniform distribution in temperature and in concentration of component B. Also the end walls are assumed to be planar at all times. Note that these boundary conditions are a subject of research in themselves (see, e.g., refs. [12,13]). Fortunately, the predicted convective flows are little influenced by the exact boundary conditions so they need not be considered further here.

The equations of the system were solved by a finite difference scheme. For the details of the computation see ref. [10].

The main result of the computation is shown in fig. 3. Here the Sherwood number (Sh) is given as a function of Gr for fixed Pr, Sc and AR. As expected, as Gr is increased, the effect of convection increases, eventually dominating the mass transfer.

The corresponding KU results are also plotted in fig. 3. The KU results level out at the Gr midrange. The numerical model, however, predicts a continuous increase in transport with increasing Grashof number, in good agreement with experimental observations [8].

Interestingly, an investigation of the effect of the Peclet number (Pe) (which is here a measure of the in-flow and out-flow velocities at the crystal and the source, respectively) on the total transport showed that it had virtually no effect. This indicates that the diffusive through-flow has a negligible effect on total velocity, even in the presence of weak convection.

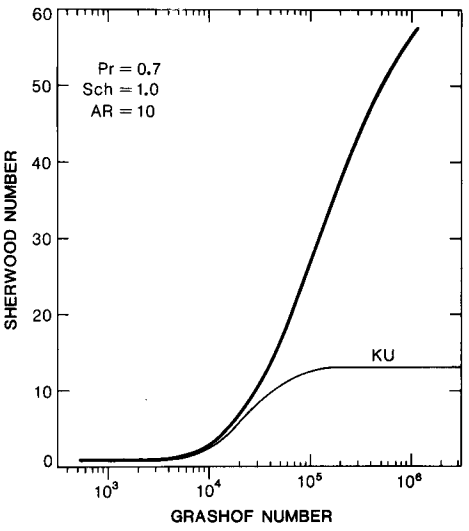

Fig. 3. Sh as a function of Gr for convective transport in a channel. After ref. [10].

KU assume a linear temperature profile in the cavity. The numerical results, however, indicate that this is true only at low Grashof numbers. Fig. 4 shows computed temperature profiles taken at half height ($y = h/2$) along the length of the cavity for an aspect ratio of 5 and three different Grashof

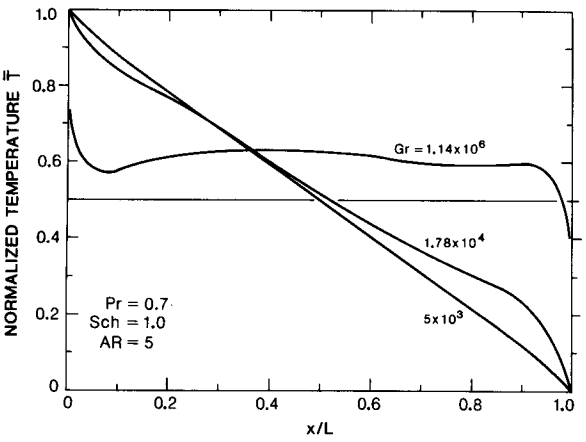

Fig. 4. Effective of Gr on temperature profile. As Gr increases, boundary layer flow develops. After ref. [10].

numbers. At $Gr = 5 \times 10^3$, where excellent agreement with the Sh predicted by KU is found, the profile is almost linear. At $Gr = 1.78 \times 10^4$, where the transport results of the two models begin to diverge significantly, the profile also begins to show convective deformation. At $Gr = 1.4 \times 10^6$ the profile is extremely deformed and has assumed a so called boundary layer type shape. Thus the numerical model predicts a transition from core driven to boundary layer driven flow, whereas, the KU model is limited, by assumption, to the core driven mechanism.

Of particular interest to the crystal grower is the growth flux distribution across the interface. The growth flux, as represented by the A component velocity, is plotted in fig. 5 as a function of y/h for an aspect ratio of 5 and four different values of Gr. In general, a higher nutrient supply is found in the upper part of the cavity, where the flow connects source and crystal more directly. In the lowest part, the flux is reduced below the diffusion only value (dashed line). Note that even for $Gr = 2 \times 10^3$, where $Sh = 2$, the flux varies by a factor of 2.4 across the interface. Thus, even when the net effect of free convection on the overall transport rate is small, convection causes a strong deviation from a uniform species distribution. It should be realized, however, that diffusion alone in viscous interaction with the side walls can cause some non-uniformity in growth flux [13–15]. For this zero body force case, the non-uniformity

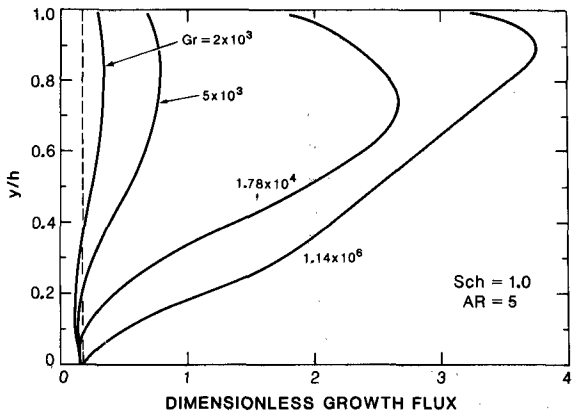

Fig. 5. Growth flux as a function of y/h. Note strong spatial nonuniformity in flux. After ref. [10].

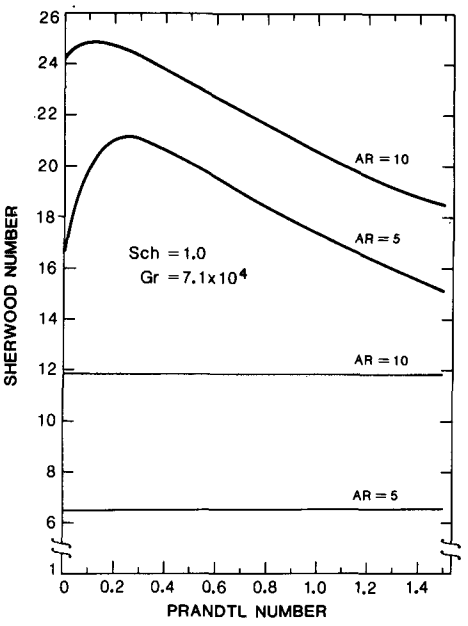

Fig. 6. Sh as a function of Pr. Transport peaks at nonzero Pr. After ref. [10].

is only a few percent. Hence, the major deformation in the flux profile observed here results from free convection.

KU (indirectly) assume a $Pr \approx 0$ throughout their analysis. The numerical model, however, shows a significant Pr dependence of the transport. Fig. 6 is a plot of Sh versus Pr for $Gr = 7.1 \times 10^4$ and aspect ratios of 5 and 10. Note that the maximum overall transport is not obtained at $Pr = 0$, where (since $\kappa \to \infty$) the temperature profile remains linear. For AR = 5, the maximum Sh lies at $Pr \approx 0.25$ and for AR = 10 at $Pr \approx 0.1$. This demonstrates that the net transport between source and crystal in the convective regime results from a balance between core-driven and boundary layer (end region) driven flow. This is further indicated by the effect of Pr on the temperature profile. As Pr increases the temperature profile is deformed so that at the higher Prandtl numbers it is flat in the area between the ends and very steep at the ends themselves. This suggests that, as Pr increases, the flow changes from core driven to boundary layer driven.

For comparison, the KU predictions are also

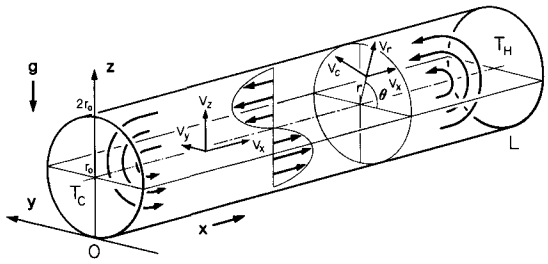

Fig. 7. Geometry investigated in laser Doppler anemometry experiments. After ref. [16].

plotted in fig. 6. Note that at Pr = 0 there is a large discrepancy in the Sh values. This illustrates the effect of the other simplifications used in the KU analysis.

For further discussion of the effect of Schmidt number, geometry, and inclination of the channel with respect to gravity on the transport, see ref. [10].

2.2. Experimental results

Armed with such a powerful tool as the foregoing analysis seemingly provides, one is now tempted to compare the model's predictions with experimental results. As pointed out in ref. [10] however, only a few vapor transport experiments have been characterized to the point that some comparison could be made. For these few examples, only semi-quantitative correlations could be obtained.

The lack of quantitative agreement is due, at least in part, to the two-dimensional nature of the model used. This is clearly illustrated by a recent paper [16] on laser Doppler anemometry studies of the (three-dimensional) convective velocity fields in closed cylinders. Laser Doppler anemometry is a technique for measuring the three components of a gas velocity with only very minor disturbances of the gas itself. The geometry investigated in ref. [16] is shown in fig. 7. The cylinder was made of fused silica and the end pieces of copper. The left end piece was held at temperature T_c and the right one at a higher temperature T_h. A linear temperature profile (as measured along the inner tube surface) was established by external heating elements. Typically, the cylinder was filled with pure nitrogen gas at pressures between 10 and 200 kPa.

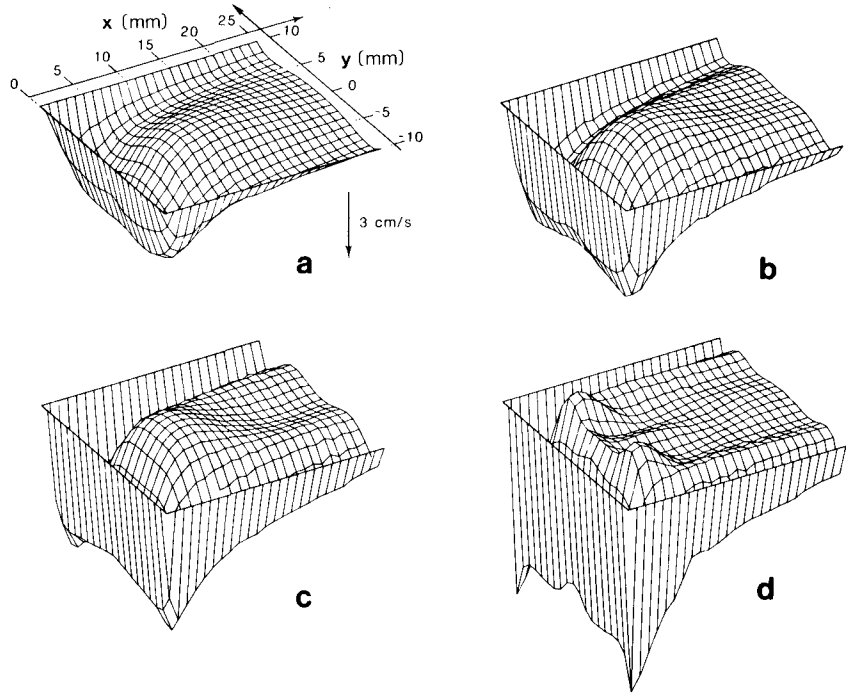

Fig. 8. Vertical velocity component V_z near cold end wall measured in the horizontal mid-plane for: (a) Ra = 3580, (b) Ra = 8860, (c) Ra = 18,700, and (d) Ra = 343,100. Same velocity scale for all figures. After ref. [16].

One of the most striking results of this work is the nature of flow near the end plates. Fig. 8 shows the measured vertical (Z) component of velocity in the horizontal midplane ($Z = r_0$) at the cold end piece. Four different Rayleigh numbers were investigated. The figure indicates that only part of the vapor flows along the cold wall ("crystal") into the lower half of the cylinder. The remaining part changes the flow direction by dropping at the side wall over a considerable distance from the end wall. Such a complex flow pattern cannot be predicted from a two dimensional analysis. Also, intuitively, the pattern implies non-uniform crystal growth. This result indicated that three-dimensional analysis, including realistic boundary conditions, are required for a quantitative investigation of vapor growth systems. The two dimensional approach, however, will remain as a useful tool in predicting trends that can lead to improvements of the transport conditions.

The state of understanding is further exasperated when one consider the vapor growth experiments in which the body force responsible for the convective drive (i.e., gravity) has been made very small. Chandra and Wiedemeier [8] have described the growth of GeSe by CVT with GeI_4 in space and on earth. They have found that in space the transport rate is 300% larger than the corresponding convectivety stable (i.e., vertical ampoule, top heated) configuration on earth. This result still defies explanation. Given this development it seems evident that further space experiments should be done with simpler (e.g., no chemical reactions) very well characterized systems such as I_2/H_2 or I_2/Ar. This will eliminate any possible chemical effects and allow concentration on the fluid dynamics of the situation.

3. Convective effects in open flow systems

3.1. Hot wall CVD reactors

By definition, there is always convection in an open flow system. The temperature gradients employed in these systems, however, usually cause buoyancy-driven convection in addition to the forced convection. In fact, it is the interplay of forced and free convection that determines the optimal operating range of a reactor.

Because the temperature gradients found in hot wall reactors are much less than those in cold wall configurations, it may be thought that buoyancy-driven convection is not a factor in hot wall growth

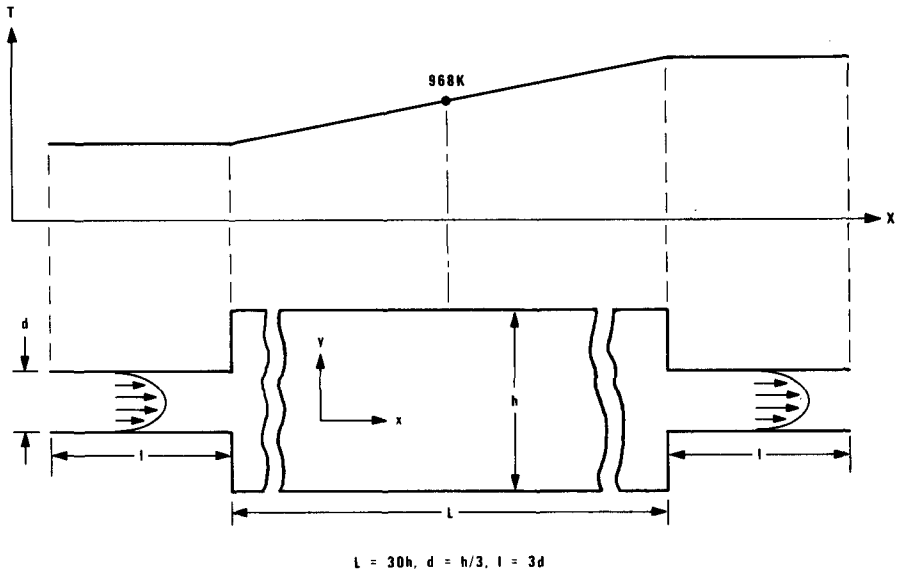

Fig. 9. Idealized geometry used to model the flow channel reactor. After ref. [17].

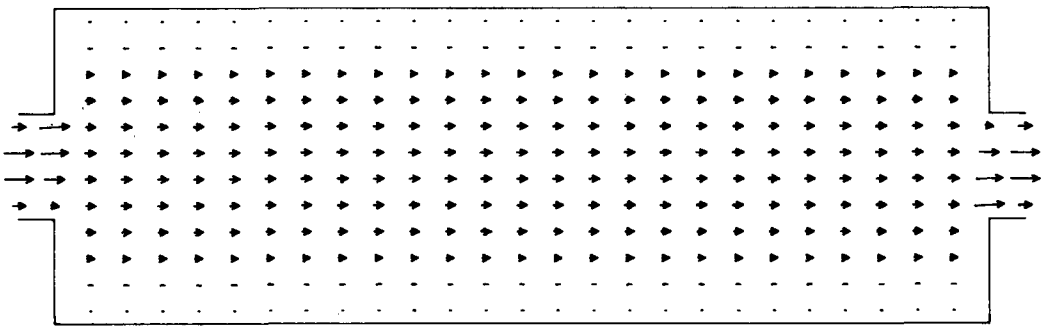

(a) h=0.1cm $\langle V_x \rangle$ = 0.25cm/sec ∇T=300.0 K/cm

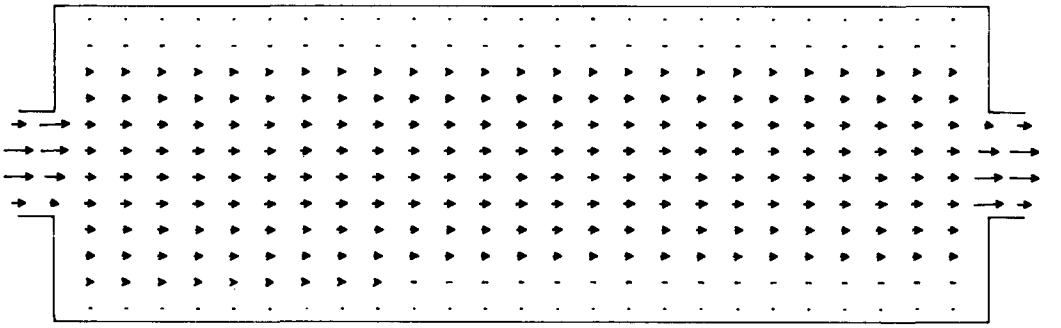

(b) h=0.5cm $\langle V_x \rangle$ =0.5cm/sec ∇T=60.0 K/cm

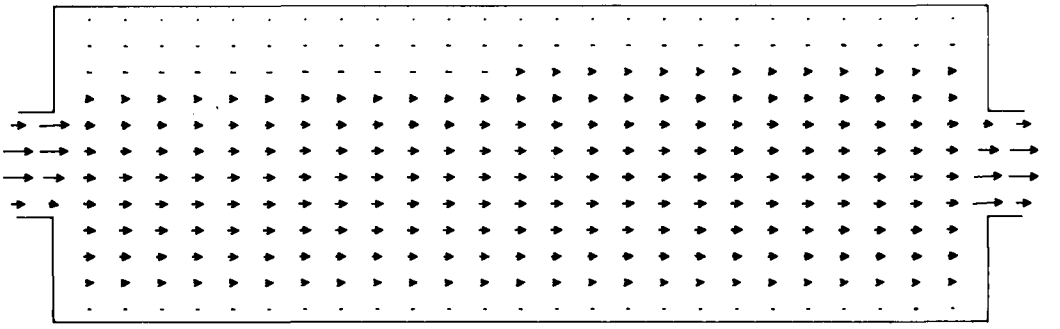

(c) h=1.0cm $\langle V_x \rangle$ =1.0cm/sec ∇T=30.0 K/cm

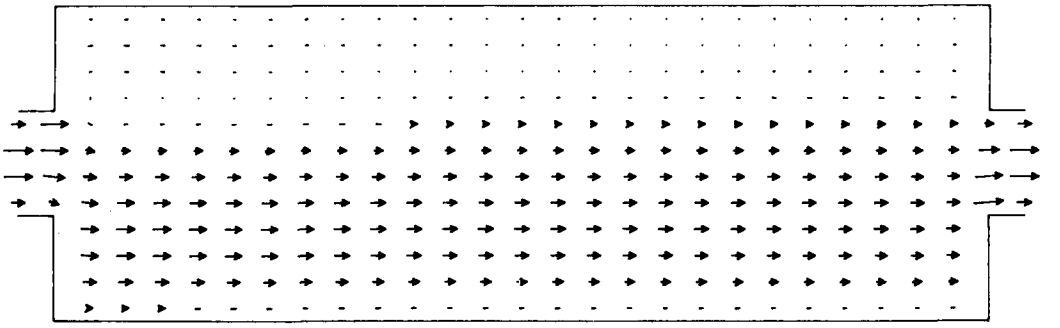

(d) h=2.5cm $\langle V_x \rangle$ =1.5cm/sec ∇T=12.0 K/cm

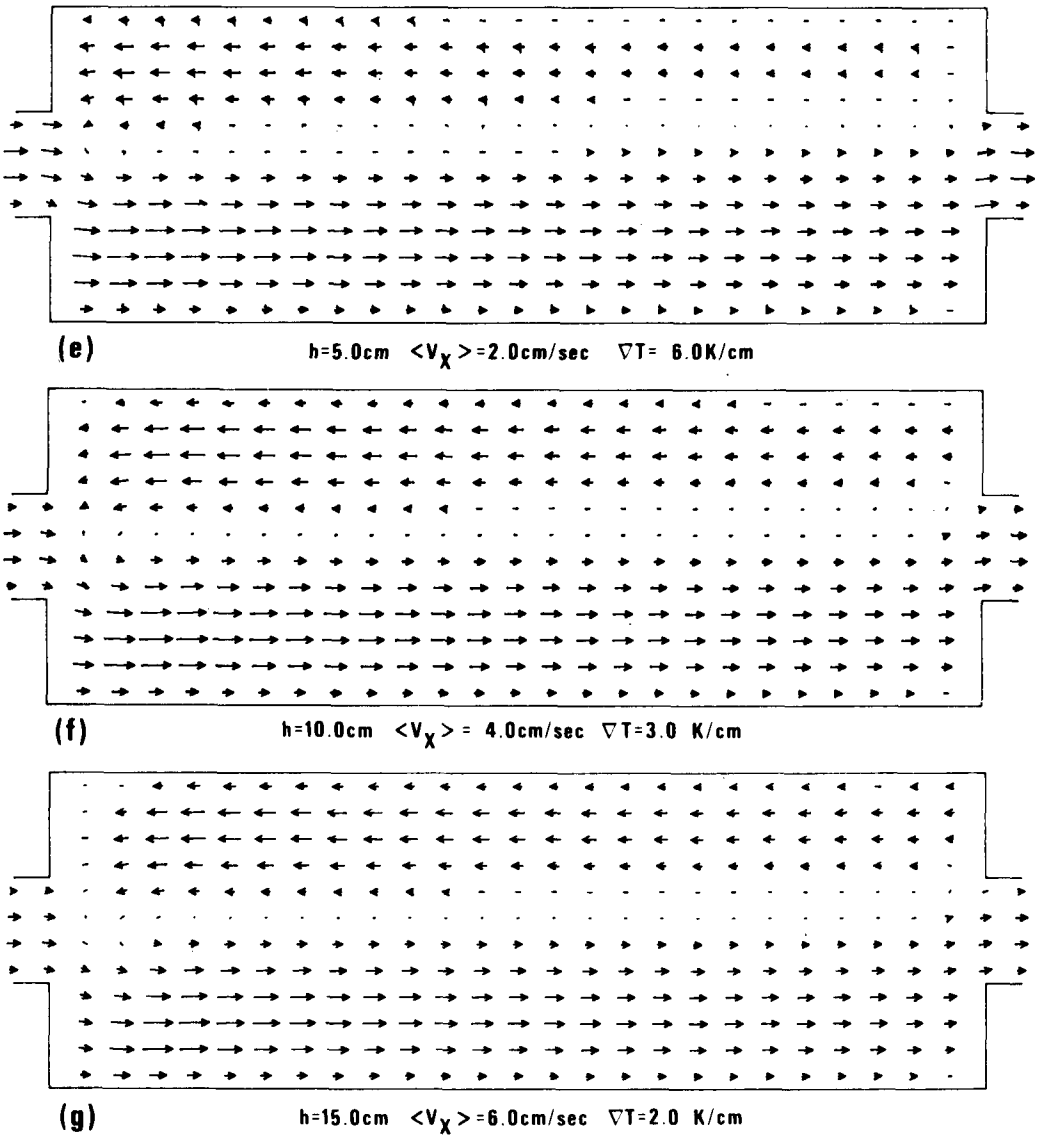

Fig. 10. Plot of the velocity field for various channels. Numerically, all channels are normalized by $\langle V_x \rangle$, which is the average x component of the fluid velocity taken along a line at the channel center perpendicular to the flow direction. After ref. [17].

(hot wall implies no radial or transverse temperature gradient). This is not the case. In the course of an investigation of the epitaxial growth of GaAs, Westphal et al. [17] have demonstrated that even small temperature gradients can cause large buoyancy-driven convective effects in large diameter reactor tubes. The geometry they investigated is shown in fig. 9. This is an idealization of the reactor, using a restricted two-dimensional rectangular channel. Note that the temperature profile used was chosen for computational convenience and is more indicative of the reactor entrance region (upstream cold, downstream hot), but the results are also valid for the typical exit region (upstream hot, downstream cold).

The fluid flow in the channel was analyzed by

application of finite difference techniques to the two-dimensional stream function vorticity formulation of the monocomponent equations of fluid dynamics, including the energy equation. Ideal gas behavior was assumed and density variations were accounted for by the Boussinesq approximation. The visocity was assumed constant and fluid properties appropriate to pure hydrogen at 100 kPa total pressure were used. An average temperature of 968 K was used for all cases. Laminar parabolic flow was assumed at the entrance and exit.

The results of the (steady state) calculations are summarized in fig. 10, which is a plot of the velocity field in the channel for various values of channel height, temperature gradient and average flow velocity, $\langle V_x \rangle$. It is reasonable to expect that the greater the average flow velocity and the smaller the temperature gradient, the smaller will be the effect of free convection. These results, therefore, demonstrate that the channel height strongly dominates the onset of free convection.

The conditions of figs. 10e, 10f, and 10g correspond roughly to conventional systems of 50, 100, and 150 mm tube diameter, respectively. Note, however, that the flow velocities are larger and the temperature gradients are smaller than are generally found in practice for such systems. The results indicate then that even the small reactors (50 mm) have significant free convection, while the larger systems are dominated by it.

One detrimental effect of the large convective cell is uncontrolled dilution of the incoming reactant stream. If a cell connects a colder downstream (exhaust) region of the tube with a hotter upstream (deposition zone) region then the (depleted) gas coming from the colder region will mix with the incoming reactant stream, diluting it and presenting a different concentration of reactants to the growth interface than would be the case in laminar flow. The dominance of convective cells over laminar flow as reactor tube diameter increases is one reason upscaling of hot wall reactors has been so problematic. The cells cannot be suppressed by simply increasing the flow rate in a typical GaAs reactor, for example, because of limitations imposed by the condensed phase source [17]. Thus, laminar flow usually can be achieved only by modification of reactor geometry.

3.2. Cold wall CVD reactors

The open flow cold wall reactor is the mainstay for the epitaxial growth of silicon. Because of the industrial importance of this process, many reactor geometries have been devised, as shown in fig. 11. The first reactor is a single wafer pedestal type used largely for laboratory work due to its low capacity. The next three reactors have all been used for production. The horizontal reactor is perhaps the most studied of the four. The barrel reactor is currently the most commonly used reactor industrially. The last reactor, the pancake type, is apparently the least well characterized of the group. The horizontal and barrel reactors are displacement reactors; that is the incoming gas sweeps out the reacted gases. In the pancake reactor the

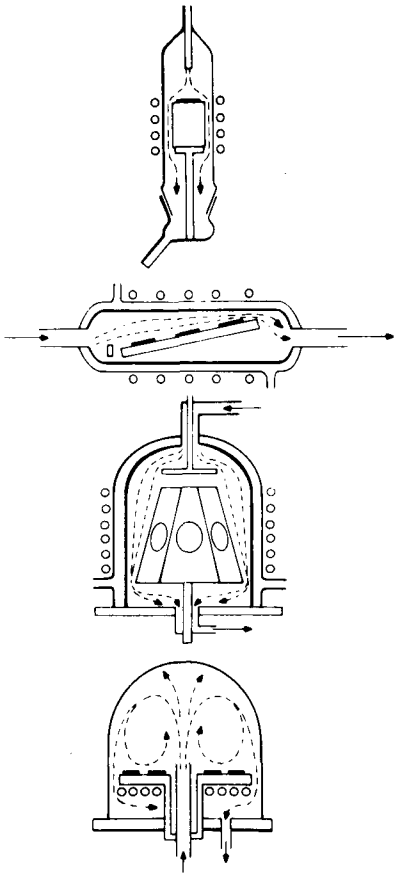

Fig. 11. Schematic representation of conventional epitaxial reactors. After ref. [19].

incoming gas partially mixes with the reacted gases. The strong recirculatory convection that occurs over the substrate provides excellent mixing and distribution of the reactants. This results in excellent layer thickness uniformity. Because of the mixing, however, it is not possible to abruptly change the gas dopant concentration and therefore, only gradual doping level transitions may be achieved in the deposited layer. Therefore, the pancake reactor is restricted to the preparation of homogeneous layers of a single material [18].

Recently [19] a new type of reactor was developed, called the rotary disc reactor. The goal of this reactor was to minimize the effects of natural convection while maximizing uniformity, throughput, and capacity. However, it apparently has not found widespread application.

"Cold wall" Si CVD reactors are so called because in normal operation a silicon slice is placed on a susceptor which is heated to, say 1200°C, while its surroundings are kept cool. A stream of gas containing a gaseous silicon compound (usually $SiCl_4$, SiH_4 or a chlorosilane in H_2) is then passed over the hot slice and solid silicon is generated by thermal decomposition. Because of the extreme temperature differences employed in these reactors, buoyancy-driven convection often plays a decisive role in the nature of gas flow near the slice and, hence, on the uniformity of the deposited layer thickness.

The mathematical description of the interaction of forced and buoyancy-driven convection is rather complex. Analytical, solutions to the complete set of equations governing the fluid flow in CVD reactors are impossible and complete numerical simulations of reactor flow are still rare. Most analysis done to date make strong simplifying assumptions and construct models involving adjustable parameters. Nevertheless, these models usually result in an adequate description of experiments, at least over some range of parameters.

Sparrow et al. [26] have used the value of Gr/Re^2 as a criterion to determine at what combinations of temperature difference and gas velocity the contribution of expansive convection becomes imporant to the gas flow for a vertical heated wall. For large values, buoyancy dominates. For small values, forced flow dominates. For values near unity, mixed flow obtains. Note that in their analysis the flow is always laminar and that their criterion is based on the contribution of the buoyancy force to that laminar flow. They never attempted to make predictions about the formation of convective cells.

The ratio Gr/Re^2 occurs naturally as a consequence of non-dimensionalizing the governing equations of heat and momentum transfer [26]. Thus, one might be tempted to consider it a universal criterion. However, two points must be made. First, there is absolutely no physical basis for generalizing a criterion devised for laminar flow near a vertical hot wall to, say, a horizontal hot wall. And second, as we will see below, there is strong evidence that the criterion does indeed not apply to the horizontal reactor.

3.2.1. The vertical pedestal reactor

The single slice vertical pedestal reactor is often used for research or small volume production. Wahl and Hoffmann [20,21] have produced an excellent hydrodynamic analysis of this reactor, using numerical simulation. The results of his work are shown in fig. 12. These results were confined experimentally with flow visualization techniques. Note that in the bottom figure (opposing flow) the effects of buoyancy-driven convection are clearly evident. The convective rolls predicted by the numerical model were clearly evident in the visualization experiments. Only flow conditions represented by the upper figure were investigated for layer thickness uniformity (in this case Si_3N_4). It was found that the layer was thickest at the center (stagnation point) and became thinner at the edges. For analysis of similar systems in which the pedestal is rotated, see refs. [22–25].

3.2.2. The barrel reactor

The models used to describe open flow systems often take a form in which buoyancy-driven convection is neglected altogether. For the barrel reactor in particular this assumption is justifiable in that the direction of the forced flow is parallel to the gravity vector. Thus, if the flow is fast enough the effect of buoyancy is small.

Examples of analysis of the barrel reactor using laminar flow are given in [27–29]. Mass transfer is

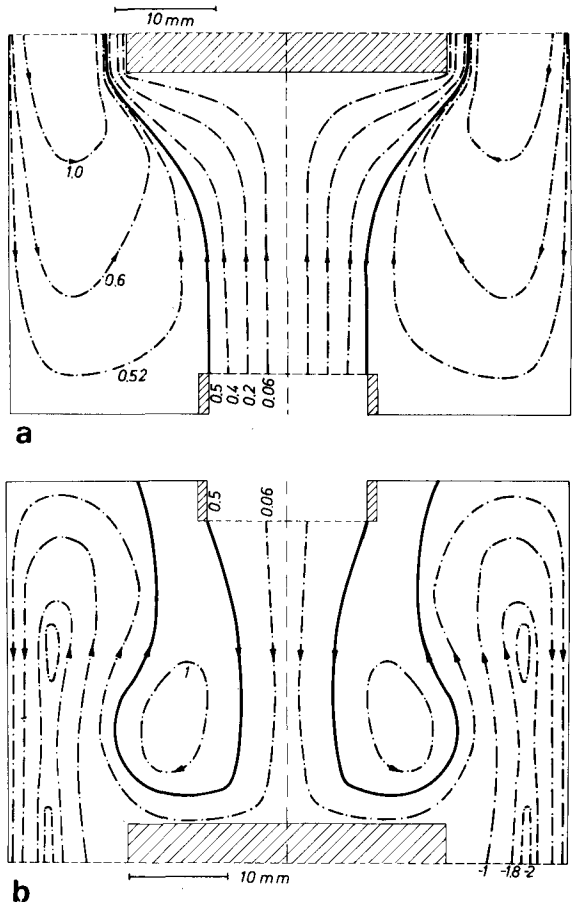

Fig. 12. Calculated flow lines for vertical pedestal reactor: Re = 50, T_d = 900 K: (a) aided flow; (b) opposing flow. After ref. [20].

analyzed by diffusion and surface chemical kinetics. In particular, the importance of thermal diffusion (Soret effect) is pointed out in ref. [24]. Because of the large temperature gradients and large molecular weight differences (between, say, H_2 and $SiCl_4$) found in silicon CVD systems thermal diffusion cannot be ignored. For additional insight into the Soret effect as it affects CVD, see refs. [30,31].

Note that the recent trend is to operate barrel reactors at reduced pressures (well below atmospheric). Under such conditions, buoyancy effects will be negligible.

3.2.3. The horizontal reactor

In the horizontal reactor, there are temperature gradients as high as 400°C/cm perpendicular to the main gas flow direction. This gives rise to some of the most significant buoyancy-driven convective effects observed in cold wall reactors.

The effects of expansive convection are best observed by flow visualization experiments. The first such experiment was performed by Eversteyn et al. [32]. TiO_2 smoke was injected into the incoming gas stream and the resulting distribution of particles was supposed to follow the flow streamlines. Thus, by taking photographs through the reactor side or end walls, the gas flow pattern could be observed for a variety of reactor conditions or susceptor temperatures and volume flow rates.

Eversteyn et al. used a water cooled rectangular cross section fused silica reactor through which hydrogen gas at 1 atm pressure was flowed. Flow velocities between 15 and 180 cm/s were used. They found that with a temperature gradient of 5°C/cm (flow rate unspecified) above a room temperature susceptor, two longitudinal vortex rolls developed, rotating at about 1 rps. With increasing susceptor temperature and vertical temperature gradient, the roll rotation rate increased and the streamlines mixed. Except at low gas velocities, there was a layer of gas just above the susceptors with a very low concentration of TiO_2 particle. Eversteyn et al concluded that this layer is a region where the gas velocity is zero and that the incoming particles flow only in a region separated from the susceptor by a "stagnant" layer. Similar observations were made by Ban and Gilbert [33] and Berkman et al. [34] except that they considered the layer near the susceptor to be in laminar flow. In both cases, the gas above the layer was considered to be well mixed.

Unfortunately, proper account was not taken in these experiments of the effect of the temperature gradient on the motion of the particles. According to Kaye [35], fineparticles (0.01 to 5 μm) placed in a thermal gradient will tend to move in the direction of lower temperature. This phenomenon is well known in industrial aerosol processing and is particularly pronounced in steep temperature gradients. Thermal precipitators based on this

principle collect fineparticles with high efficiency.

Beyond these considerations, one can apply some basic physics to the situation. By definition a (Newtonian) fluid cannot support a shear. For there to be a stagnant layer of gas some 5 mm thick near the wall at the axial center of a long tube in which the free stream velocity is on the order of 100 cm/s is physically impossible. There is no stagnant layer.

A flow visualization technique complementary to particle injection is interference holography. Using this approach, Giling [36] has provided a thorough qualitative analysis of the horizontal reactor. He studied the flow patterns of H_2, He, N_2, and Ar at a variety of flow rates and susceptor temperatures, in circular and rectangular cross section reactors with both air and water cooled walls.

The result of this technique is a gas density map of the reactor cross section in the form of a photographic plate in which constant density contours are shown as fringes. This map may be time dependent. Because the gas density is also temperature dependent, the fringe patterns are subject to interpretation. In general, however, when the gas flow is stable and laminar the temperature profile will be stable and the fringe pattern will be fixed in time. If there is unsteady convection in the gas, then the fringe pattern will be time dependent. If there is turbulence in the gas, then the local temperature will change rapidly and the pattern will be blurred.

Figs. 13 and 14 are typical of Giling's results for H_2 and He in an air cooled cylindrical reactor. At the lower flow velocity (fig. 13) parallel fringes are observed near the susceptor (the dark rectangular area at the bottom). Near the top of the tube the fringes curve toward the susceptor. The pattern is stable in time. At the higher flow velocities (fig. 14) closed concentric rings appear, but the pattern is still time independent. These circular fringes become more dominant as the susceptor temperature increases or its length decreases. These results indicate that basically laminar flow prevails under the reactor conditions investigated.

The circular fringes are interpreted as a "cold finger" or region of lower gas temperature. This result has also been observed by Ban [41] who measured temperature profiles above the susceptor in a horizontal reactor using a thermocouple.

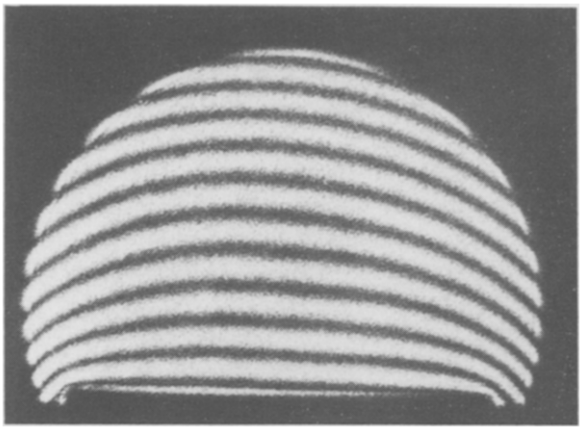

Fig. 13. Interference pattern for H_2 (He), $V = 10$ cm/s air cooled cylindrical cell, $T_{susc} = 1350$ K, susceptor length = 20 cm. After ref. [36].

Giling's results should be compared to the partical flow visualization experiments of Takahashi et al. [37,38] and Sugawara et al. [30]. As mentioned above, the particle approach does not give valid results near the susceptor where the temperature gradients are extreme, but are generally valid in the main flow of the reactor. Takahashi investigated lower flow velocities for He than Giling. At the lower velocities, spiral vortex rolls were clearly evident. As the velocity was increased the rolls gradually disappeared until laminar flow pre-

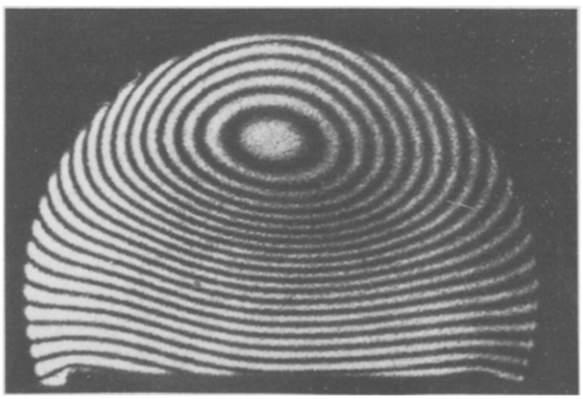

Fig. 14. Fringe pattern for H_2(He), $V = 70$ cm/s air cooled cylindrical cell, $T_{susc} = 1350$ K. susceptor length = 20 cm. After ref. [36].

vailed. At very high velocities a shaded region in the tube center developed corresponding to Giling's concentric rings. Note that Sugawara et al. [39] found a deposition pattern corresponding to the vortex rolls when Si was deposited by reaction of $SiCl_4$ with H_2 at low flow rates. The deposition pattern was very non-uniform indicating that the gas was not well mixed by the rolls. For further discussion of the development of longitudinal rolls, see ref. [40].

Giling found that for H_2 or He in a water cooled cylindrical reactor the ring fringes could not be generated at any flow velocity. Also the fringes tended to bend strongly toward the susceptor. In a top (water) cooled rectangular reactor, however, very parallel fringes were found.

For N_2 and Ar, a large variety of convective effects were observed. These gases proved to be much less stable than H_2 or He. Typically the fringe pattern showed a strong time dependence. In all cases, a laminar flow region, where thickness varied with time and location, developed near the susceptor. Above this region various complex. often turbulent, flows dominated. These results are similar to those obtained by Takahashi et al. [38] for N_2.

Giling [36] has noted some basic differences between the water-cooled and air cooled reactors. He has measured the quartz wall temperature to be between 600 and 900 K for the air-cooled reactor. This is much higher than for the water-cooled case. The cold gas finger mentioned above occurs only in the air-cooled case and indicates a much higher gas velocity in the region of the concentric fringes, than in the same region in the water-cooled reactor. This is because of a large expansion of the gas near the hot wall together with a higher gas viscosity in the hotter region. Because of the higher viscosity the gas velocity near the wall will be lower than normal. But the mean velocity is fixed by the input flow. Therefore, the core velocity must increase in order to maintain the same mean velocity. This creates a more severe entrance effect (see below) which appears as the cold finger.

Giling's work also clearly demonstrates that Sparrow's criteria ref. [26], see above) for flow characterization does not apply to the horizontal reactor. Indeed no correlation was observed in Gilling's experiments between the ratio Gr/Re^2 and convective stability. For example, no characteristic difference is noted between the ratio values for H_2 and N_2, but H_2 gives a stable laminar flow and N_2 a highly unstable "mixed" flow.

3.3. Convective instability

Flow through an isothermal channel can be classified by the Reynolds number (Re) as laminar or turbulent according to whether $Re < 2300$ or $Re > 3200$, respectively [42]. At a free stream velocity of 120 cm/s and with an average gas temperature of 1000 K and a channel height of 2.5 cm, $Re = 260$ for N_2 or Ar, and $Re = 30$ for He or N_2 [36]. According to this criterion, turbulent effects are not to be expected for any of the gases under typical reactor conditions. Yet there is clear evidence for some turbulent motion of the gas, even for H_2 under conditions where the holography measurements [36] found none. This turbulence is revealed by time dependent temperature measurement in typical reactors. In particular Ban [41] found temperature oscillations in He with a

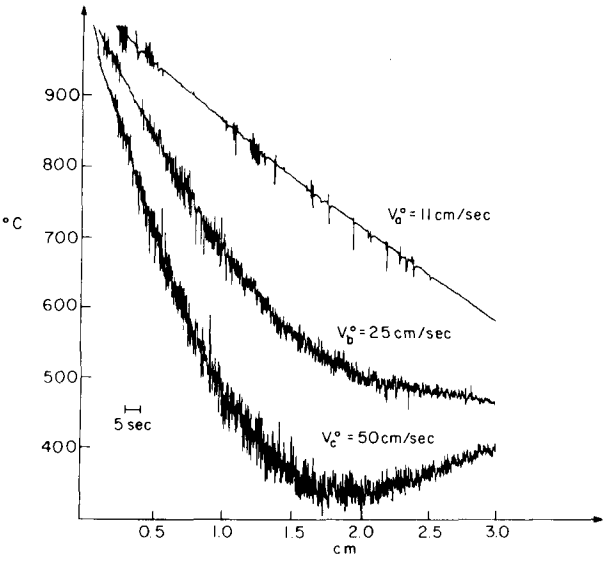

Fig. 15. Direct recording of temperature profiles in He showing oscillations, $T_{susc} = 1000°C$, measurement was taken 15 cm from susceptor leading edge. After ref. [41].

frequenccy of about 1 Hz at distances greater than about 2.5 mm from the susceptor surface in a horizontal reactor. At a flow velocity of 11 cm/s, the oscillations were sporadic and not well developed. However, at 25 cm/s oscillations were present in the whole space above the susceptor and had amplitudes of about 25°C. At 50 cm/s the amplitudes were about 75°C. As the oscillations increased in amplitude, the cold finger described above also developed. Ban's results are summarized in fig. 15. Note that Giling found a perfectly time stable fringe pattern under the same reactor conditions.

Curtis and Dismukes [43] have also found temperature oscillations in the barrel reactor. However, in a vertical pedestal reactor, the same authors [46] could not find oscillations in H_2 under any conditions. Oscillations were found for He. For further discussion of these observations, see refs. [44,45,48]. For a review of the corresponding effects of convective instability and temperature oscillations in closed systems, see refs. [1,8,44,45].

Ban [41] also analyzed the concentration distribution of $SiCl_4$ above the susceptor using mass spectroscopy. He found steep concentration gradients near the susceptor similar to the steep temperature gradients. In addition, however, he found oscillations in the concentration, again of about 1 Hz in frequency. These oscillations occurred throughout the entire space above the susceptor.

The convective state of a gas in an enclosed volume subjected to a destablizing temperature gradient (hot on bottom, cold on top) is characterized by the Rayleigh number (Ra). As Ra increases, progressively more complex modes of flow develop, transistions usually taking place at a series of specific Ra's, depending on fluid properties and geometry. (For further discussion of these transitions, see Krishnamurti [46].).

Use of Ra to characterize an open flow system is perhaps questionable, but it does seem to correlate well with the tendency of a system to show mixed convection rather than pure laminar flow. For example, at a susceptor temperature of 1000 K and a channel height of 2.5 cm, Ra = 100 for H_2 or He and Ra = 5800 for N_2 or Ar [36]. To the extent that the above mentioned trend can be transferred to the open flow case, N_2 and Ar will be much less convectively stable than H_2 or He, just as observations indicate. For an explanation of the stability of the laminar layer near the susceptor seen for N_2 and Ar, see Giling [36].

Curtis and Dimukes [44] have shown that for many gases Ra is proportional to p^2T^{-m} where p is the total gas pressure, T the mean gas temperature and $4.3 < m < 4.8$. Thus the gas becomes more stable as T increases and p decreases. The latter effect was clearly demonstrated by Takahashi et al. [38] in that laminar flow in their reactor was achieved at low velocities at reduced pressures.

Finally it must be noted that flow in horizontal reactors is subject to entrance effects. According to Schlichting [42] the velocity profile in an isothermal channel of height, h, is fully developed after an entrance length of $x = 0.04\ h$ Re. At 1000 K and for $h = 2.5$ cm and a free stream velocity of 40 cm/s, $x = 1.1$ cm for He and H_2 and $x = 9.0$ cm for N_2 and Ar. Thus for the latter gases, the velocity profile is changing over a large fraction of the susceptor length. Note that the actual length for the non-isothermal case may be somewhat different than the one just calculated.

The temperature profile is also subject to entrance effects. Hwang and Cheng [47] have shown that for a horizontal parallel-plate channel heated from below, the thermal entrance length is $x = 0.40\ h$ Pr Re $= 0.28\ h$ Re for gases with Pr = 0.7. Thus, the thermal entrance length is 7 times that of the velocity profile. Thus even for H_2 and He, if the flow velocity exceeds 10 cm/s, significant axial variations in temperature will be found. These predictions have been experimentally confirmed by Ban [41] and Kamotani and Ostrach [48].

3.4. Mass transport and growth rate calculations

A number of models have been constructed for the description of mass transport in cold wall horizontal CVD Si reactors. The earliest of these [49–51] dealt only with equilibrium calculations and considered the reactors as a closed box. Anticipating Eversteyn, Bradshaw [52] assumed the existence of a static layer of gas immediately above the susceptor surface through which reactants diffuse to an equilibrium region at the substrate

surface. This model works well for systems where the deposition efficiency is low. Shephard's parallel plate theory [53] assumes fully developed parabolic laminar flow in the reactor, but does not allow for a variation of concentration in the direction of gas flow. Rundle [54] does allow for such a variation but assumes "plug" flow (flow velocity constant throughout the reactor).

Several models assume plug flow over a stagnant layer near the interface. Eversteyn et al. [32] use a simple version while Bloem [55] adds thermal diffusion and Van den Brekel [56] treats surface kinetics as well. An excellent summary of these early models is given by Bloem and Giling [57].

Takahashi et al. [37] have given a thorough numerical analysis of the effect on deposition of vortex rolls. For the laminar flow case, they have attempted a three dimensional analysis of the concentration field.

Berkman et al. [34] have based an analysis of mass transport on the observations of Ban [33,41]. This analysis is based on traditional hydrodynamic boundary layer models. Gilings results [36] however, make clear, especially for well developed flows of H_2 and He, that no boundary layer exists in the sense that Berkman, et al., use it. But note that the existence of temperature and concentration oscillations [41] in what are apparently well developed flows is still without adequate explanation.

The most complete model for mass transport in a Si CVD system with laminar flow is that of Juza and Cermak [28]. They calculate the velocity, temperature and concentration profiles and take account of both thermal diffusion and surface kinetics. Note that all of these models predict depletion of reactants in the gas phase in the flow direction, with a resulting decrease of growth rate downstream. This effect is confirmed experimentally and has led to the common practice of tilting the susceptor in order to achieve a constant axial growth rate.

Often, both surface kinetics and gas mass transfer must both be considered to achieve an adequate description of the growth rate. If the susceptor temperature is low enough however, then the growth rate for CVD Si will be limited by the surface kinetics and gas phase mass transfer will play a secondary roll. For examples of analysis in which the surface kinetics dominates, see Aoyama et al. [58] and Korec [59].

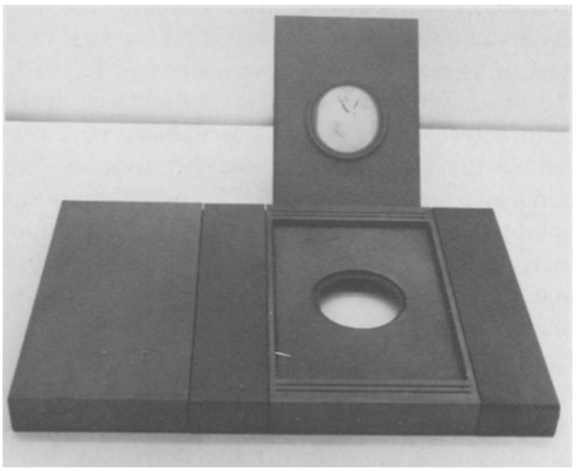

Fig. 16. Slice carrier used in CCVD reactor.

3.5. The continuous CVD reactor (CCVD)

The CCVD reactor [60] is an example of how convective effects can be used to advantage in thin film deposition.

The reactor consists of a series of chambers through which a single slice susceptor or carrier is passed. Each chamber has an independent gas flow associated with it. The carrier, shown in fig. 16 has a channel-like in cross section (see fig. 17).

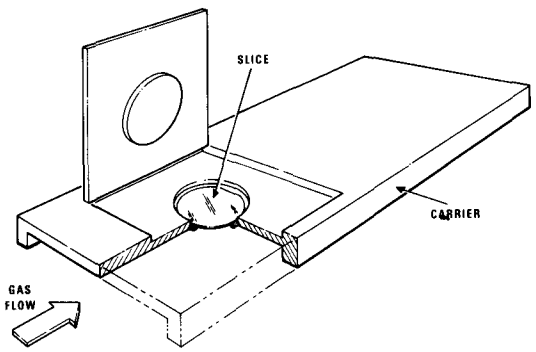

Fig. 17. Cross sectional drawing of slice carrier showing gas channel.

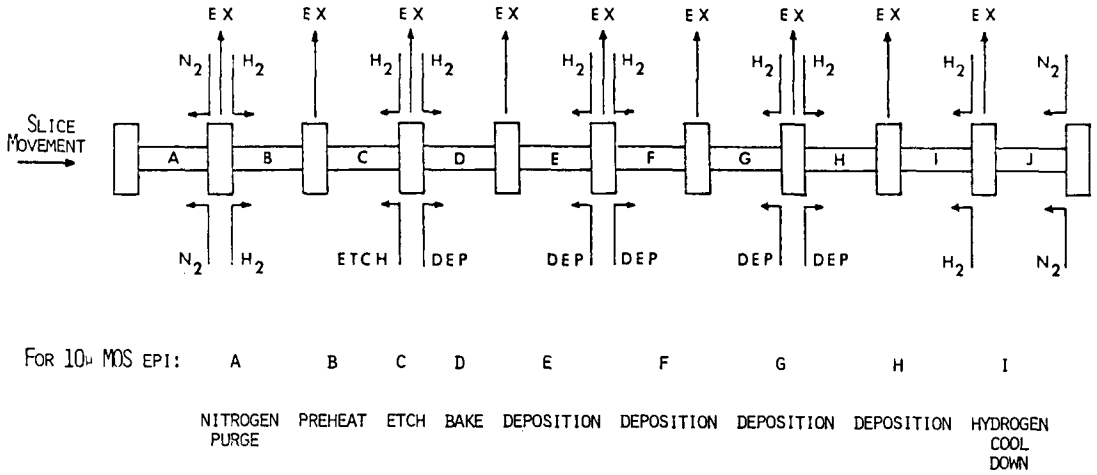

Fig. 18. Schematic representation of chambers in the CCVD reactor.

The slice is mounted face down and when the carrier is in a chamber, gas flows through the channel of the carrier and across the slice face. The carrier is optically heated from above, so to first order, the system is convectively stable and laminar flow prevails. As noted above this leads to wedge-shaped growth since the growth rate falls off downstream. However, with this reactor that effect can be countered easily. If growth if performed in "paired" chambers (see fig. 18), each with a gas flow direction opposite to the other, then wedge growth in the first chamber will compliment the growth in the second and a uniform layer will result. This is what is experimentally observed.

4. Summary

Despite the very elegant analysis that has been done, the state of our knowledge of convective effects in vapor growth systems is still, in many ways, primitive. In closed tube systems, rarely are the physico-chemical properties of the vapors characterized well enough to make optimum use of the fluid dynamic models available. These models themselves, being mostly two-dimensional, are often inadequate for a quantitative account of reality, but serve only as qualitative guides. This situation is graphically illustrated by Chandra and Wiedemeier's result [8] showing anomalously high transport rates in a low gravity environment.

The situation is similar in open tube systems. The nature of the chemistry and surface kinetics in Si CVD systems is still a subject of controversy, judging by the recent literature [58,59]. That Ban [41] finds turbulent temperature oscillations under conditions that Giling [36] calls time stable laminar flow indicates a poor general understanding of convection in these systems.

Several areas of future work are indicated. First, apperently three-dimensional modeling is going to be essential to a quantitative understanding of many important systems. Obviously, three-dimensional experiments, similar to the work in ref. [16], will be needed to verify the models. Also thorough physico-chemical evaluation of the systems of interest is needed.

Beyond this, the above mentioned contradictions point up a fundamental lack of understanding of convective effects. This is demonstrated most clearly be the lack of an adequate criterion for the transition from buoyancy driven to forced convection in open flow systems.

Nomenclature

AR Aspect ratio $= l/h$

C_p Heat capacity per gram at constant pressure

D_{AB} Binary diffusivity
Gr Grashof number = $\beta g \Delta T h^4 / \nu^2 l$
g Acceleration due to gravity
h Channel height
k Thermal conductivity
l Channel length
Pe Peclet number = Vh/D_{AB}
Pr Prandtl number = ν/κ
Ra Rayleigh number = $\beta g \Delta T h^3 / \kappa \nu$
Re Reynolds number = Vh/ν
Sh Sherwood number = area averaged mass flux to a surface normalized by the one-dimensional flux
Sc Schmidt number = ν/D_{AB}
T Temperature
$\tilde{T}$ Reduced temperature = $[T - T(l)]/[T(0) - T(l)]$
V Fluid velocity
β Coefficient of thermal expansion
η Dynamic visocity
κ Thermal diffusivity = $k/\rho C_\rho$
ν Kinematic viscosity = η/ρ
ρ Mass density

References

[1] F. Rosenberger, Physico-chem. Hydrodyn. 1 (1980) 3.
[2] M. Krulfeld, Mater. Res. Bull. 2 (1967) 337.
[3] F. Rosenberger, Fundamentals of Crystal Growth I (Springer, New York, 1979).
[4] A. Solan and S. Ostrack, in: Preparation and Properties of Solid State Materials, Vol. 4 (Dekker, New York, 1979).
[5] F. Rosenberger, in: Convective Transport and Instability Phenomena, Eds. J. Zierep and H. Oertel, Jr. (Braun, Karlsruhe, 1982).
[6] K. Klosse and P. Ullersma, J. Crystal Growth 18 (1973) 167.
[7] C. Paorici and C. Pelosi, J. Crystal Growth 35 (1976) 65.
[8] D. Chandra and H. Wiedemeier, J. Crystal Growth 57 (1982) 159.
[9] B.S. Jhaveri and F. Rosenberger, J. Crystal Growth 57 (1982) 57.
[10] B.L. Markham and F. Rosenberger, J. Crystal Growth submitted.
[11] R.B. Bird, W.E. Stewart and E.N. Lightfoot, Transport Phenomena (Wiley, New York, 1960).
[12] R. Jackson, Transport in Porous Catalysts (Elsevier, New York, 1977).
[13] D.W. Greenwell, B.L. Markham and F. Rosenberger, J. Crystal Growth 51 (1981) 413.
[14] B.L. Markham, D.W. Greenwell and F. Rosenberger, J. Crystal Growth 51 (1981) 426.
[15] B.L. Markham and F. Rosenberger, Chem. Eng. Commun. 5 (1980) 287.
[16] G.H. Schiroky and F. Rosenberger, Intern. J. Heat Mass Transfer, in press.
[17] G.H. Westphal, D.W. Shaw and R.A. Hartzell, J. Crystal Growth 56 (1982) 324.
[18] B.J. Curtis, Physico-Chem. Hydrodyn. 2 (1981) 357.
[19] V.S. Ban, J. Crystal Growth 45 (1978) 97.
[20] G. Wahl, Thin Solid Films 40 (1977) 13.
[21] G. Wahl and R.H. Hoffmann, Rev. Intern. Hautes Temp. Réfract. 17 (1980) 7.
[22] K. Sugawara, J. Electrochem. Soc. 119 (1972) 1749.
[23] M.L. Hitchman and B.J. Curtis, Progr. Crystal Growth and Characterization 4 (1981) 285.
[24] M.L. Hitchman, B.J. Curtis, H.R. Brunner and V. Eichenberger, in: Physico-Chemical Hydrodynamics, Vol. II, Ed. D.B. Spalding (Advance Publications, 1977) p. 1021.
[25] M.L. Hitchman and B.J. Curtis, J. Crystal Growth 60 (1982) 43.
[26] E.M. Sparrow, R. Eichhorn and J.L. Gregg, Phys. Fluids 2 (1959) 319.
[27] E. Fuji, H. Nakamura, K. Haruna and Y. Koga, J. Electrochem. Soc. 119 (1972) 1106.
[28] J. Juza and J. Cermak, J. Electrochem. Soc. 129 (1982) 1627.
[29] C.W. Manke and L.F. Donaghey, J. Electrochem. Soc. 124 (1977) 561.
[30] P. van der Putte, L.J. Giling and J. Bloem, J. Crystal Growth 31 (1975) 299.
[31] D.E. Rosner, Physico-Chem. Hydrodyn. 1 (1980) 159.
[32] F.C. Eversteyn, P.J. W. Severin, C.H. van den Brekel and H.L. Peek, J. Electrochem. Soc. 117 (1970) 925.
[33] V.S. Ban and S.L. Gilbert, J. Crystal Growth 31 (1975) 284.
[34] S. Berkman, V.S. Ban, and N. Goldsmith, in: Heteroepitaxial Semiconductors for Electronic Devices, Eds. G.W. Cullen and C.C. Wang (Springer, Berlin, 1978) p. 264.
[35] B.H. Kaye, Direct Characterization of Fineparticles (Wiley–Intersience, New York, 1981).
[36] L.J. Giling, J. Electrochem. Soc. 129 (1982) 634; J. Physique 43 (1983) C5-235.
[37] R. Takahashi, Y. Koga and K. Sugawara, J. Electrochem. Soc. 119 (1972) 1406.
[38] R. Takahashi, K. Sugawara, Y. Nakazawa and Y. Koga, in: Chemical Vapor Deposition, Proc. 2nd Intern. Conf., Eds. J.M. Blocher and J.C. Withers (Electrochem. Soc., New York, 1970) p. 695.
[39] K. Sugawara, R. Takahashi, H. Tochikubo and Y. Koga, in: Chemical Vapor Deposition, Proc. 2nd Intern. Conf., Eds. J.M. Blocher and J.C. Withers (Electrochem. Soc., New York, 1970) p. 713.
[40] S. Ostrach and Y. Kamotani; in: Heat Transfer and Turbulent Buoyant Convection, Vol. 2, Eds. D.B. Spalding and W. Afgan (Hemisphere, 1977).
[41] V.S. Ban, J. Electrochem. Soc. 125 (1978) 317.
[42] H. Schlichting, Boundary Layer Theory, 6th ed. (McGraw-Hill, New York, 1968) p. 177.

[43] B.J. Curtis and J.P. Dismukes, in: Proc. 4th Intern. Conf. on Vapor Deposition, 1973, Eds. G.F. Wakefield and J.M. Blocher, p. 218.
[44] B.J. Curtis and J.P. Dismukes, J. Crystal Growth 17 (1972) 128.
[45] J.P. Dismukes and B.J. Curtis, in: Semiconductor Silicon 1973, Eds. H.R. Huff and R.R. Burgess (Electrochem. Soc., New York, 1973) p.250.
[46] R. Krishnamurti, J. Fluid Mech. 42 (1970) 295.
[47] G.J. Hwang and K.C. Cheng, J. Heat Transfer 95 (1973) 72.
[48] Y. Kamotani and S. Ostrach, J. Heat Transfer 98 (1976) 62.
[49] W. Steinmaier, Philips Res. Rept., 81 (1963) 75.
[50] R.F. Lever, IBM J. Res. Develop. 8 (1964) 466.
[51] M.J. Harper and T.J. Lewis, Ministry of Aviation ERDE Technical Memorandum 6/M/66 (1966).
[52] S.E. Bradshaw, Intern. J. Electrochem. 21 (1966) 205.
[53] W.H. Shepherd, J. Electrochem. Soc. 112 (1965) 988.
[54] P.C. Rundle, Intern. J. Electron. 24 (1968) 405.
[55] J. Bloem, J. Electrochem. Soc. 117 (1970) 1397.
[56] C.H.J. van den Brekel, Philips Res. Rept. 31 (1977) 118; C.H.J. van den Brekel and J. Bloem, Philips Res. Rept. 32 (1977) 134.
[57] J. Bloem and L.J. Giling, in: Current Topics in Materials Science, Vol. 1, Ed. E. Kaldis (North-Holland, Amsterdam, 1977) p. 147.
[58] T. Aouama, Y. Inoue and T. Suzuki, J. Electrochem. Soc. 130 (1983) 203.
[59] J. Korec, J. Crystal Growth 61 (1983) 32.
[60] D. Bellavance and R.N. Anderson, J. Electrochem. Soc. 130 (1983) 101C.